

Modelling supercapacitors using a dynamic equivalent circuit with a distribution of relaxation times

L.E. Helseth

Department of Physics and Technology, Allegaten 55, 5020 Bergen, University of Bergen, Norway

ABSTRACT: Supercapacitors are often modelled using electrical equivalent circuits with a limited number of branches. However, the limited number of branches often cannot explain long-term dynamics, and one therefore has to resort to more computationally challenging basic models governing diffusion and drift of ions. Here, it is shown that consistent modelling of a supercapacitors can be done in a straightforward manner by introducing a dynamic equivalent circuit model that naturally allows a large number or a continuous distribution of time constants, both in time and frequency domains. Such a model can be used to explain the most common features of a supercapacitor in a consistent manner. In the time domain, it is shown that the time-dependent charging rate and the self-discharge of a supercapacitor can both be interpreted in this model with either a few or a continuous distribution of relaxation times. In the frequency domain, the impedance spectrum allows one to extract a distribution of relaxation times. The unified model presented here may help visualizing how the distribution of relaxation times or frequencies govern the behavior of a supercapacitor under varying circumstances.

KEYWORDS: Supercapacitor, modelling, distribution of relaxation times.

1. Introduction

Electrochemical double layer capacitors, often called supercapacitors, were patented in 1957 and later commercialized [1,2]. Supercapacitors are based on porous carbon immersed in an electrolyte, where the ions can form an electrical double layer which aids in storing electrical charge. The large number of pores, often with a large size distribution, results in charge dynamics covering a hierarchy of time scales. Modelling of supercapacitors must take into account this distribution of time scales.

Supercapacitors are often modelled using equivalent circuits composed of resistors and capacitors, including inductive elements which may become important at higher frequencies, both in the time and frequency domains [3-17]. An early transmission line model of porous electrodes in electrolytes in Ref. [18] was later shown to be consistent with molecular dynamics simulations [19], and this model has been used to understand the behavior of supercapacitors as well [20,21]. Representing a supercapacitor in terms of an equivalent circuit composed of passive elements is not only a convenient and computationally efficient method to describe the supercapacitor, it is also based on sound physics. Indeed, linearization of the partial differential equations describing the system results in linear ordinary differential equations that can be associated with a passive electrical network [22,23]. Comparisons have been made between the equivalent circuits to better understand their performances [24-26], and multiscale models have been shown to represent impedance spectra well [27]. Methods for accurate fitting of model parameters are needed [28], and recursive algorithms have been used to obtain better fits to experimental data characterizing charge-discharge cycles [29].

Various means to follow the online dynamics and improve power management during use of the supercapacitor may involve real time equivalent circuit parameter estimation [30], Kalman filtering [31,32], and variable capacitor models [33] to allow better online power management. However, also further understanding of the underlying equivalent models are needed. Fractional order calculus provides a method for more accurately modelling the supercapacitor performance [34-37]. However, it should also

be pointed out that standard electrical circuit analysis can be utilized to a fuller extent in order to interpret experimental data. In Ref. [38] it was suggested how one may model a supercapacitor using a number of serial RC-circuits arranged in parallel in terms of a distribution of time constants in frequency domain, and how the finite Pascal equivalent circuits could be used to interpret results. Ref. [39] demonstrates how the relaxation of frequencies can be used to extract information about degradation of supercapacitors from impedance spectra. However, the distribution of relaxation times found in impedance spectra of supercapacitors is often very narrow, and it would be advantageous to also have a suitable description in the time domain such that charging and self-discharging phenomena also could be described. In the current work it is shown how to model a supercapacitor using a number of parallel RC circuits in series, the so-called dynamic equivalent circuit, in order to extract the equivalent distribution of relaxation times, both in time and frequency domains. The distribution of relaxation times can be utilized to visualize the slow and fast charge dynamics in a supercapacitor, and may also be a useful tool when designing new systems. Thus, the current work is a natural expansion of previous studies, and should further the understanding of how to model supercapacitors using electrical equivalent circuits.

2. The dynamic equivalent circuit

The circuits considered in this work are shown in Fig. 1. Figure 1 a) shows a Randle circuit, which is often used to model the simplest features of supercapacitors. It consists of a resistor (R_p) and capacitor (C_p) in parallel, connected to a serial resistor (R_s). To explain the high frequency behavior (typically above 100 Hz), an inductor of inductance L is added. However, the inductive behavior is often related to the metallic cover of the supercapacitor and may not play a role in understanding the supercapacitor itself. This circuit has a single relaxation time, and therefore represents only a limited set of the mobile charges in a supercapacitor. Nonetheless, it is often a reasonable approximation when trying to model the supercapacitors in a limited temporal or frequency range, although in particular self-discharge cannot be understood using such a circuit.

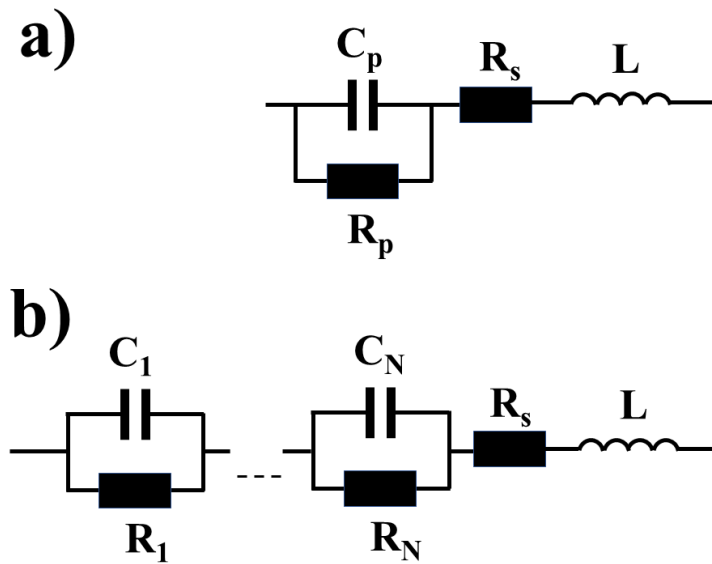


Figure 1. Equivalent electrical circuits representing a supercapacitor. In a), a Randle circuit is shown, whereas b) shows the dynamic circuit.

The dynamic equivalent circuit in Fig. 1 b) can be rationalized by linearization of the partial differential equations describing diffusion, drift, charge conservation [23]. It is composed of a series of parallel resistors and capacitors, which allows one to incorporate multiple time constants when modelling the supercapacitor. In principle, any continuous distribution of time constants can be generated, but this potential appears to not yet have been fully exploited. In the following an approach to model all important aspects of supercapacitors using the model in Fig. 1 b) is presented.

3. Experimental details

In this study, two different supercapacitors were studied, hereafter named A and B. Supercapacitor A was a GoldCap of nominal capacitance 10 F and voltage limit 2.5 V. Supercapacitor B was made by Ioxus, of nominal capacitance 400 F and voltage limit 2.7 V. The measurements of voltage, current and impedance were done with either a Biologic SP050 or a Gamry Ref. 600. Currents of 0.1 A, 0.5 A or 0.8 A were

provided during galvanostatic charging, where the fluctuations were kept below ± 0.1 mA. The voltage fluctuations were typically about ± 0.1 mV. The galvanostatic impedance spectroscopy was run between 2 mHz and 1 MHz with 50 mA root-mean-square about zero average current.

4. Galvanostatic charging

Galvanostatic charging of a supercapacitor is made by applying a constant current I_0 while measuring the voltage V_C over the capacitor as function of time. The dynamic equivalent circuit model in Fig. 1 b) is used as the starting point when extracting information from the experimental data. The supercapacitor is charged by a constant current I_0 which is the same through all elemental parallel circuit parts and given by

$$I_0 = I_{C_i} + I_{R_i} = \frac{dQ_i}{dt} + \frac{Q_i}{R_i C_i}, \quad (1)$$

where the current through the capacitor C_i is $I_{C_i} = dQ_i/dt$ and the current I_{R_i} through the resistor R_i was found by noting that the voltage over C_j and R_j are equal and can be given by

$$\frac{Q_i}{C_i} = R_i I_{R_i}. \quad (2)$$

Equation (1) above can be solved to give the following equation for the charge on capacitor C_i :

$$Q_i(t) = Q_i(0)e^{-t/\tau_i} + I_0 \tau_i (1 - e^{-t/\tau_i}), \quad \tau_i = R_i C_i. \quad (3)$$

Here $Q_i(0)$ is the initial charge and τ_i the relaxation time for one particular elemental circuit branch. So far, only one elemental circuit branch (resistor and capacitor in parallel) has been considered, although it is a fact that in a supercapacitor one would have a large number of such elements. From a statistical point of view, one could say that there is a distribution of relaxation times τ_i , or equivalently that there is a

certain probability that each elemental circuit with relaxation time τ_i is excited. Therefore it is convenient to assign a weight α_i to each initial charge $Q_i(0)$, such that there is a probability α_i that the charge $Q_i(0)$ is present on the elemental branch of relaxation time τ_i . Also the current passing through the elemental branches follows a statistical distribution, since the particular branch of relaxation time τ_i may allow current to pass through or not, depending on whether there is any blockage due to for example small sized-pores or an electron tunneling layer or other factors controlling the current in that branch. From a statistical point of view, there is a probability β_i that the current I_0 runs through the elemental circuit with relaxation time τ_i . It should be pointed out that the two weight factors fulfill $\sum_{i=1}^N \alpha_i = 1$ and $\sum_{i=1}^N \beta_i = 1$ to ensure that the total probability sums up to one. From Eq. (3), the total charge gained by the supercapacitor after a time t is given by

$$Q(t) = \sum_{i=1}^N Q_i(t) = \sum_{i=1}^N \alpha_i Q_i(0) e^{-t/\tau_i} + I_0 \sum_{i=1}^N \beta_i \tau_i (1 - e^{-t/\tau_i}) \quad . \quad (4)$$

For small times, $t \ll \tau_i$, in absence of initial charge it is seen that $Q(t) \approx I_0 t$, as also obtained using the Randle circuit in Fig. 1 a). If one neglects the inductor, the voltage $V_C(t) = \sum_{i=1}^N \frac{Q_i}{C_i} + R_s I_0$ over the entire supercapacitor is given by

$$V_C(t) = \sum_{i=1}^N \alpha_i V_i(0) e^{-t/\tau_i} + I_0 \sum_{i=1}^N \beta_i R_i (1 - e^{-t/\tau_i}) + R_s I_0 \quad , \quad (5)$$

where $V_i(0) = Q_i(0)/C_i$ is the initial voltage over capacitor C_i . The voltage rate is given by

$$\frac{dV_C(t)}{dt} = \sum_{i=1}^N \left[\beta_i \frac{I_0}{C_i} - \alpha_i \frac{V_i(0)}{\tau_i} \right] e^{-t/\tau_i} \quad . \quad (6)$$

Equations (4) and (5) constitute the results of the discrete part of the model presented here. This discrete model allows one to use any finite number of relaxation times τ_i to model the system at hand. Using Eqs. (4) and (5) requires prior knowledge about the distribution functions α_i and β_i . Alternatively, one could extract information about these distributions from the experimental data. Upon initial charging, the voltage makes a jump $R_s I_0$ before the time-dependency proceeds according to the two first terms in Eq. (5). This current-dependent jump is also observed experimentally for the supercapacitors considered here, in consistency with other previous studies under different circumstances [40]. However, the current-dependent initial voltage jump is besides the main point of this work, and therefore not considered further.

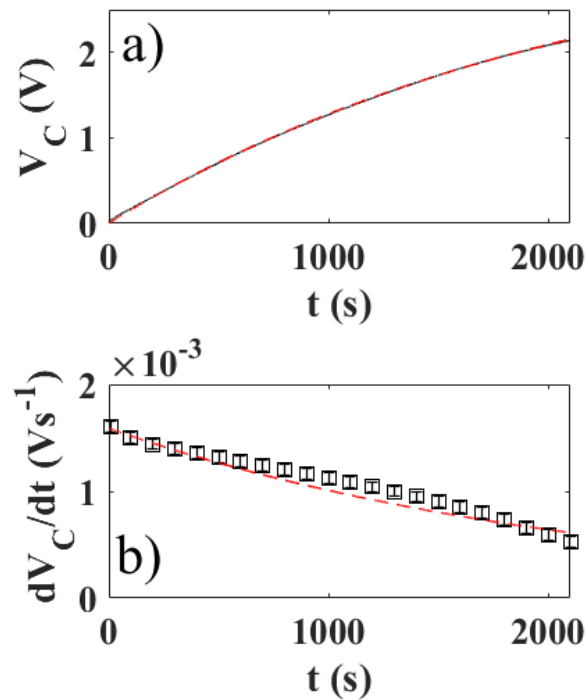


Figure 2. The voltage (a) and voltage rate (b) over supercapacitor B is shown as a function of time when supercapacitor B is charged at a constant current 0.5 A. The dashed red lines in (a) and (b) corresponds to a fit of Eqs. (5) and (6) to the experimental data with $C_1=343$ F and $\tau=2200$ s.

The black solid line in Fig. 2 a) represents the experimental voltage data obtained during galvanostatic charging of supercapacitor B at $I_0=0.5$ A, while the dashed red line corresponds to a fit of Eq. (5) to the experimental data with $N=1$, $C_1=343$ F and $\tau=2200$ s. The R^2 value of 0.9998 suggests that the fit is very good. The voltage rate extracted from the experimental data is shown in Fig. 2 b) as boxes, and a fit of Eq. (6) to the experimental data is presented as a dashed red line. The R^2 value of the fit is 0.9352, and is therefore not as accurate as the voltage fit in Fig. 2 a). Nonetheless, the fact that the voltage and voltage rate are described very well by Eqs. (5) and (6) with only $N=1$ elemental circuit branch may at first sight suggest that a single relaxation time plays the most important role here. However, it should also be mentioned that the voltage rate in Fig. 2 b) is nearly linear. In the case of $t \ll \tau_i$ for all contributing elemental branches and $V_i(0)=0$, one may write Eq. (6) as $dV_C/dt=a-bt$, where $a = \sum_{i=1}^N \beta_i I_0 / C_i$ and $b = \sum_{i=1}^N \beta_i I_0 / \tau_i C_i$. Here, it is clearly seen that the slope remains nearly linear even when there are contributions from more than one branch. Thus, with a nearly linear slope one cannot definitely conclude whether it is only one or several relaxation times present.

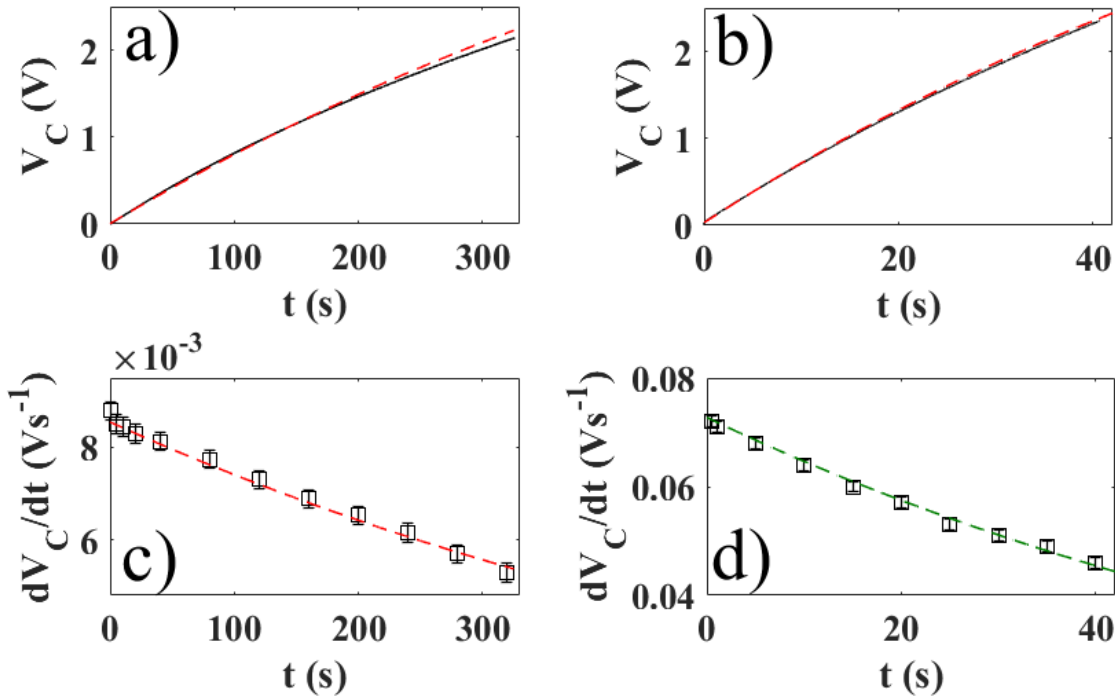


Figure 3. In a) and c), the voltage and voltage rate over supercapacitor A is shown as a function of time when supercapacitor A is charged at a constant current 0.1 A. The dashed red line corresponds to a fit of Eqs. (5) and (6) to the experimental data with $N=1$, $C_1=11.7$ F and $\tau=700$ s. In b) and d), the voltage and voltage rate over the supercapacitor A is shown as a function of time when it is charged at a constant current 0.8 A. The dashed red and green lines correspond to fits of Eqs. (5) and (6) to the experimental data with $N=1$, $C_1=11.0$ F and $\tau=85$ s.

The black solid lines in Figs. 3 a) and b) represents the experimental voltage data obtained during galvanostatic charging of the nominal 10 F supercapacitor with $I_0=0.1$ A and $I_0=0.8$ A, respectively. The boxes in Figs. 3c) and d) are the corresponding voltage rates. The dashed red lines in Fig. 3 a) and c) correspond to fits of Eqs. (5) and (6) to the experimental data with $N=1$, $C_1=11.7$ F and $\tau=700$ s. The dashed red and green lines in Fig. 3 b) and d) correspond to fits of Eqs. (5) and (6) to the experimental data with $N=1$, $C_1=11.0$ F and $\tau=85$ s. From Fig. 3 is seen that the voltage once more is well represented by Eq. (5) with $N=1$, as exemplified by R^2 values of 0.9876 (b) and 0.9934 (d). However, since the voltage rate is nearly constant, one cannot make a definite conclusion that only one relaxation time is present. It is also seen that the fitted relaxation time decreases by a factor of 8 when increasing the current from 0.1 A to 0.8 A. At the same time, the capacitance C_i remains nearly constant as fixed by the initial slope of the curves (I_0/C_i). In our dynamic equivalent circuit model, this means that only the resistance R_i decreases significantly with current. In the dynamic equivalent circuit model of Fig. 1 b), this can be interpreted as the probability of charging a branch of a given relaxation time τ_i depends on the current. Smaller current means a higher probability of charging an elemental branch with large relaxation time, whereas larger current corresponds to small relaxation time. This phenomenon is due to the different time scales involved when filling the charge from the fast and slow branches associated with the pore structures, where large pores are filled quicker than the smaller ones. The conducting nanostructures are more or less randomly aligned in the electrolyte, and the capacitance may increase with up to three orders of magnitude as the

filler fraction increases [38]. On the other hand, the resistance may change with six orders of magnitude [38], thus suggesting that R_i has a significantly larger range than C_i in Eq. (5). The currents in the experimental data analysed are not very large for several reasons. For the experimental data investigated, it was found that currents changing by a factor of 8 (from 0.1 A to 0.8 A) did not result in any functional difference in the voltage and its derivative versus time (Fig. 3), while the nonlinear behavior changed slightly due to change in relaxation time as predicted by the Eqs. (5) and (6). Only one branch was needed to describe the experimental data. While even higher currents may give even smaller relaxation times and even couple in more than one branch, the instruments available only allowed currents up to 0.8 A. The main aim of this study is to present a new method for analysis of experimental data from supercapacitors, and due to costs and time it was not found possible to cover all cases experimentally.

Upon discharging, the delivered charge decreases with applied current in a fixed time interval, a phenomenon that has been coined Peukert's law [41]. A similar phenomenon associated with galvanostatic charging can be interpreted in terms of the dynamic equivalent circuit model used here. If the relaxation time τ_i decreases with increasing current I_0 , then Eq. (4) predicts that the charge deposited on the supercapacitor during galvanostatic charging should become smaller with increasing current. To see this, one may expand Eq. (4) to second order and obtain $Q(t) = I_0 t - \frac{1}{2} I_0 t^2 \sum_{i=1}^N \beta_i / \tau_i$. If τ_i decreases with the current, it is seen that the second term in the expansion increases monotonously with current, such that the total deposited charge decreases monotonously with current.

Equations (4) and (5) are derived assuming that there are a finite number of elemental circuit branches describing the system. While this appears to work well for the two supercapacitors considered here, other systems may behave differently. One may in principle encounter situations where a continuous distribution of relaxation times would better describe the supercapacitor. That is, during charging one encounters a large number of possible time constants and initial charge distributions, leading to a statistical distribution represented by $\alpha(\tau)$ and $\beta(\tau)$. One requires normalization such that $\int_0^\infty \alpha(\tau) d\tau =$

1 and $\int_0^\infty \beta(\tau)d\tau = 1$. Note that the continuous variables $\alpha(\tau)$ and $\beta(\tau)$ have units s^{-1} . If one assumes that the number N is very large, a continuous distribution can be assumed. It is assumed that one can let $\tau_i \rightarrow \tau$, $\alpha_i Q_i(0) \rightarrow \alpha(\tau)Q_0$, $\alpha_i V_i(0) \rightarrow \alpha(\tau)V_0$, $\beta_i \rightarrow \beta(\tau)$ and $R_i \rightarrow R_p(\tau)$ such that

$$Q(t) = Q_0 \int_0^\infty \alpha(\tau)e^{-t/\tau}d\tau + I_0 \int_0^\infty \beta(\tau)\tau(1 - e^{-t/\tau})d\tau \quad , \quad (7)$$

and

$$V_C(t) = V_0 \int_0^\infty \alpha(\tau)e^{-t/\tau}d\tau + I_0 \int_0^\infty \beta(\tau)R_p(\tau)(1 - e^{-t/\tau})d\tau + R_s I_0 \quad . \quad (8)$$

In the case of a single relaxation time τ_0 , one may write $\alpha(t)=\delta(\tau-\tau_0)$, $\beta=\delta(\tau-\tau_0)$ and $R_p(\tau_0)=R_p$, such that

$$Q(t) = Q_0 e^{-t/\tau_0} + I_0 \tau_0 (1 - e^{-t/\tau_0}) \quad (9)$$

and

$$V_C(t) = V_0 e^{-t/\tau_0} + I_0 R_p (1 - e^{-t/\tau_0}) + R_s I_0 \quad , \quad (10)$$

in agreement with what one obtains by setting $N=1$ in Eqs. (4) and (5). It should be emphasized that Eqs. (4) and (5) represent the discrete version of the theory which is more useful for describing galvanostatic charging when the deviations from ideal behavior is rather small (i.e. dV_C/dt is nearly constant) or there is a main relaxation time governing the charging. On the other hand, Eqs. (7) and (8) represent the

continuous version of the theory which might find use for describing charging situations where there is stronger nonlinear behavior due to a continuous distribution of relaxation times.

5. Self-discharging

Self-discharging is another important physical phenomenon exhibited by supercapacitors. The same framework as for galvanostatic charging can be applied, but now with $I_0=0$. From Eq. (5) the voltage over the supercapacitor is in the discrete version given by

$$V_{CD}(t) = \sum_{i=1}^N \alpha_i V_i(0) e^{-t/\tau_i}, \quad (11)$$

which upon assuming a continuous distribution of relaxation times becomes

$$V_{CD}(t) = V_0 \int_0^{\infty} \alpha(\tau) e^{-t/\tau} d\tau \quad . \quad (12)$$

By changing to a dimensionless variable in the frequency domain such that $s=1/f^*\tau$ and $P(s)=\alpha(1/f^*\tau)/f^*s^2$, this expression can be written as

$$V_{CD}(t) = V_0 \int_0^{\infty} P(s) e^{-sf^*t} ds \quad . \quad (13)$$

Equation (13) is recognized as an inverse Laplace transform, and one needs to determine the spectrum $P(s)$ in order to determine the distribution of relaxation times.

The stretched exponential function, of the form $e^{-(f^*t)^\beta}$, with β and f^* constants, was introduced by Kolrausch to explain the discharge of a capacitor (Leyden jar), after finding that a simple exponential decay did not explain the experimental data [42]. Later, it was applied to numerous physical situations where a sum of exponential relaxations were present [43-45]. In Ref. [46] a stretched exponential function $\exp(-\sqrt{t/\tau_2})$ was used, corresponding to $\beta=1/2$ conjectured from diffusion dynamics, to explain long-time discharging of the supercapacitor. However, it is not obvious why only $\beta=1/2$ dictated by diffusion alone should govern the dynamics of self-discharge, and a further investigations of improved data fitting should be guided by the available experimental data. The general stretched exponential function is a good candidate for describing the time dynamics of the voltage,

$$V_{CD}(t) = V_0 e^{-(f^*t)^\beta} = V_0 \int_0^\infty P(s, \beta) e^{-s f^* t} ds \quad . \quad (14)$$

Note that the $P(s, \beta)$ can be interpreted as probability distribution in the frequency domain (or rate constants), and that $\int_0^\infty P(s, \beta) ds = 1$. The constant f^* has units s^{-1} , but cannot be given a general interpretation in terms of a relaxation frequency as explained in ref. [45]. In the case of a single relaxation time $\tau_0=1/f^*$, $\beta=1$ and $P(s, \beta)$ is a Dirac delta function centered on τ_0 .

By setting $f^*t=x$ in Eq. (14), the Laplace transform is given by

$$P(s, \beta) = \frac{1}{2\pi i} \int_{-i\infty}^{+i\infty} e^{-(x)^\beta} e^{sx} dx \quad . \quad (15)$$

This can also be transformed into Fourier transform upon suitable change of variables, and in a few cases including $\beta=0.5$, analytical solutions exist [44,45]. For arbitrary values of the coefficient in the range $0<\beta<1$, there are several methods for evaluating it numerically [44].

The solid line in Fig. 4 a) shows the measured self-discharge of supercapacitor A after first charging it to $V_0=2.2$ V, and then measuring the voltage in absence of any current ($I_0=0$). The blue, dotted line in Fig. 4 a) shows a fit of Eq. (14) to the experimental data using $\beta=0.5$ as in Ref. [46]. The fit is better than obtained using a simple exponential decay, but there are deviations as signified by the R^2 value of 0.970. A better fit using the function *nlinfit* in MatLab is obtained using $\beta=0.4$ (red, dashed line) and $f^* \approx 6.9 \cdot 10^6$ Hz, obtaining an R^2 value of 0.997. The blue, dotted line in Fig. 4 b) is the probability density function $P(s,\beta=0.5)$, whereas the dashed red line corresponds to $P(s,\beta=0.4)$. The spectrum in Fig. 4 b) corresponding to $\beta=0.4$ (red, dashed line) has maximum value at $s_{\max}=0.060$, which corresponds to a relaxation time $\tau_{\max}=1/s_{\max}f^* \approx 2.4 \cdot 10^6$ s. This parameter does not have a very distinct physical interpretation since the spectrum is very broad. However, one can conclude that the relaxation times involved in self-discharge are much longer than those involved in galvanostatic charging events described in the previous section. Clearly, application of smaller currents may result in larger relaxation times during galvanostatic charging, but one cannot expect these to be as large as those observed during self-discharge for any practically relevant charging currents. The reason is simply that galvanostatic charging is a process constantly driven out of equilibrium, whereas self-discharge is a relaxation towards equilibrium. On a general basis, it is observed that when $\beta<1$, the probability density is shifted to larger relaxation times (or shorter relaxation frequencies), which means that there are more elemental circuit branches with larger relaxation times than expected for fast galvanostatic charging processes. Decreasing β from 0.5 to 0.4 enhances the shift to larger relaxation times.

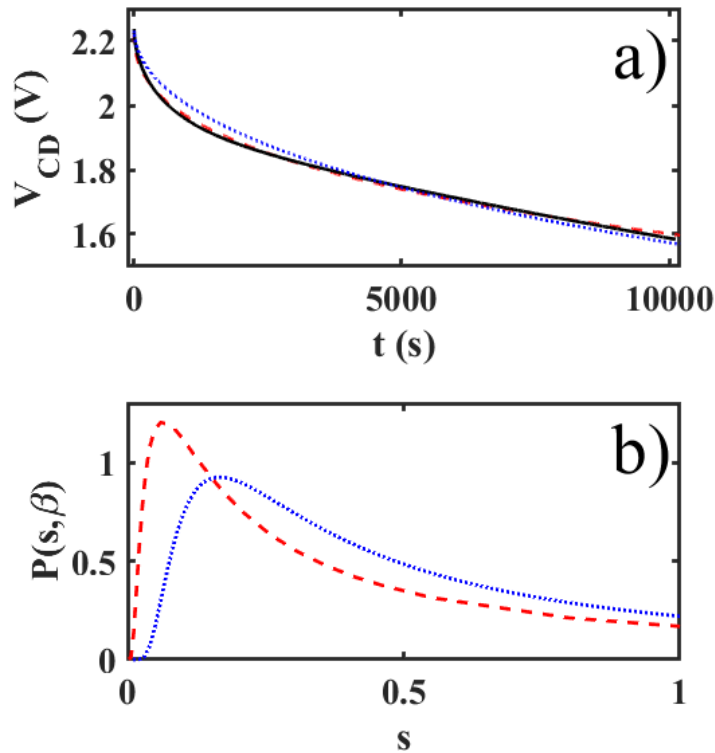


Figure 4. In a) the experimental data for the voltage over supercapacitor A during self-discharge are shown as a black, solid line. A fit with Kolrausch exponents $\beta=0.5$ (blue, dotted line) and $\beta=0.4$ (red, dashed line) give R^2 values of 0.970 and 0.997, respectively. In b), the distributions of rate constants are shown for $\beta=0.5$ (blue, dotted line) and $\beta=0.4$ (red, dashed line).

Similar trends were observed for supercapacitor B, which was first galvanostatically charged to 2.4 V followed by voltage-measurements in absence of any current ($I_0=0$). The solid line in Fig. 5 a) shows the experimental data, whereas the dashed, red line shows the best fit of the stretched exponential function to the experimental data using *nlinfit* in MatLab. One obtains $\beta=0.34$ and $f^* \approx 2.5 \cdot 10^{-6}$ Hz with R^2 value 0.987. In Fig. 5 b), the distribution function is shown for $\beta=0.34$ and $\beta=0.5$.

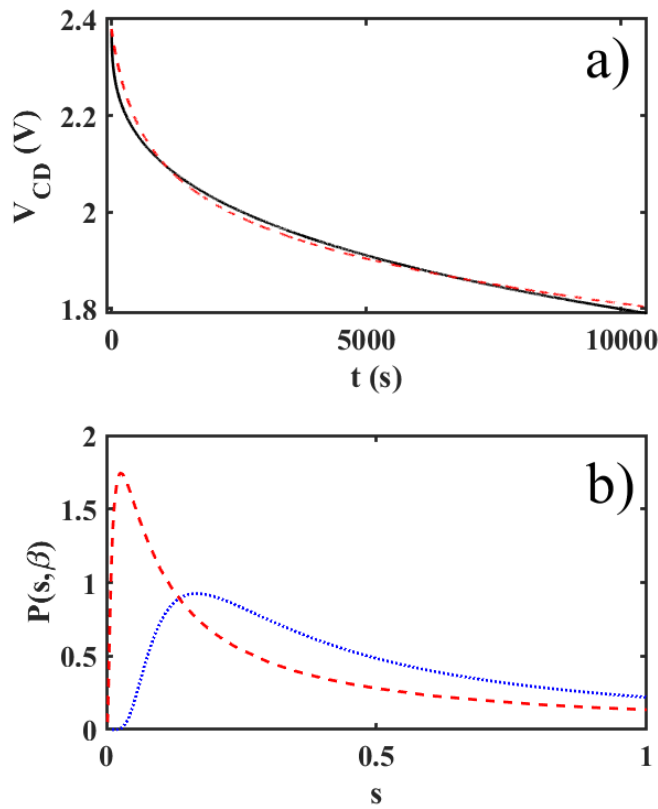


Figure 5. In a) the experimental data for the voltage over supercapacitor B during self-discharge are shown as a black, solid line. A fit with Kolrausch exponents $\beta=0.4$ (red, dashed line) give R^2 value of 0.987. In b), the distributions of rate constants are shown for $\beta=0.5$ (blue, dotted line) and $\beta=0.34$ (red, dashed line).

Note that supercapacitor B exhibits a more significant shift towards larger relaxation times (smaller frequencies) as compared to supercapacitor A, since the latter has a higher β . This could be due to a wider distribution of pores in the larger supercapacitor, but also redox-reactions may play a role. The experimentally observed self-discharge in supercapacitors can be related to ohmic losses and redox reactions [47,48], but internal redistribution of charge has been found to play a significant role [20,49-52]. Memory effects in supercapacitors are often associated with charge redistribution and have been associated with an increased resistance of ions moving in nanoporous structures [53]. A blocking layer

may alter the self-discharge due to electron tunneling, thus providing a method to control the self-discharge, often at the cost of reduced capacitance [54,55]. Self-discharge can also be used as a diagnostic tool, and has been found to be faster than conventional tools such as potential floating when determining the stability of supercapacitors based on ionic liquids [56]. At this moment it is unclear whether one could connect the distribution function $P(s,\beta)$ to geometrical parameters of the pores of the supercapacitor, which is a topic outside the scope of the current work. Nonetheless, one may be able to use the knowledge about the fitted constant β and the distribution function $P(s,\beta)$ as a diagnostic tool for analyzing self-discharging since it allows one to distinguish between distribution of relaxation times or frequencies. As such, it is different and may complement the already existing diagnostic tools based on for example polynomial fitting [57].

6. Impedance spectroscopy

In the frequency domain, the dynamic equivalent circuit in Fig. 1 b) is once again assumed. If the resistance and capacitance of the i th elements are R_i and C_i , respectively, each parallel circuit has impedance $R_i/(1+j\omega R_i C_i)$, where $j = \sqrt{-1}$. From a statistical point of view, there is a distribution of relaxation times, and a probability γ_i that current runs through a circuit of a particular relaxation time τ_i . One must require $\sum_{i=1}^N \gamma_i = 1$ to ensure that the total probability sums up to one. The total impedance of a circuit consisting of N series-connected elements is then

$$Z = R_s + \sum_{i=1}^N \frac{\gamma_i R_i}{1+j\omega\tau_i} \quad , \quad (16)$$

where R_s is the series resistance. Later we will also include the inductance L and the impedance term $j\omega L$ to account for the high frequency behavior. Now, it is convenient to define a new variable θ_i such that

$\sum_{i=1}^N \gamma_i R_i = R_p \sum_{i=1}^N \theta_i$, where R_p is a constant which in the case of a simple parallel circuit is just the parallel resistance in Fig. 1. Here, θ_i is a combination of distribution of relaxation times as well as the distribution of parallel resistors R_i . In general, θ_i and γ_i may exhibit different behavior. However, previous studies have indicated that the capacitance associated with nanograins may vary with up to three orders of magnitude, whereas the corresponding resistance may change with six orders of magnitude, thus suggesting that R_i has a significantly larger range than C_i . Under such conditions, the probability θ_i may follow the behavior of γ_i since it is mainly the values of R_i that determine the distribution of relaxation times.

If one assumes that the number N is very large, a continuous distribution can be assumed. Under such circumstances one may write Eq. (16) as

$$Z = R_s + R_p \int_0^{\infty} \frac{\theta(\tau)}{1+j\omega\tau} d\tau \quad , \quad \int_0^{\infty} \theta(\tau) d\tau = 1 \quad . \quad (17)$$

This equation can also be used to describe Debye-relaxation of dipole moments in molecules [58], and has been used to describe degradation of supercapacitors [39], batteries or fuel cells [59]. Moreover, it can also be used to describe a supercapacitor model consisting of parallel circuits [38], as opposed to the serial circuits described here. However, the interpretation in terms of the dynamic equivalent circuit given here is slightly different from previous approaches, and it is mainly introduced to complement and compare with the time-dynamic approach constructed from Fig. 1 b) and presented in the previous sections. The real and imaginary parts of Eq. (17) can be written as

$$Z_{Re} = R_s + R_p \int_0^{\infty} \frac{\theta(\tau)}{1+(\omega\tau)^2} d\tau \quad \text{and} \quad Z_{Im} = -\omega R_p \int_0^{\infty} \frac{\tau\theta(\tau)}{1+(\omega\tau)^2} d\tau \quad . \quad (18)$$

The modulus is $|Z| = \sqrt{Z_{Re}^2 + Z_{Im}^2}$ and the phase is $\phi = \tan^{-1}[Z_{Im}/Z_{Re}]$. In previous works, various methods for inverting Eq. (17) in order to obtain the statistical distribution of relaxation times have been considered [59]. In the situation where there is only one relaxation time, $\theta(\tau)=\delta(\tau_0)$, with $\tau_0=R_pC_p$, one obtains for the equivalent circuit in Fig. 1 a):

$$Z_{Re} = R_s + \frac{R_p}{1+(\omega\tau_0)^2} \quad , \quad Z_{Im} = -\frac{\omega\tau_0R_p}{1+(\omega\tau_0)^2} \quad . \quad (19)$$

To account for statistical variations that is fairly easy to model, it is convenient to assume a gaussian statistical distribution of relaxation times with standard deviation σ ,

$$\theta(\tau) = \frac{1}{\sqrt{2\pi\sigma^2}} e^{-\frac{(\tau-\tau_0)^2}{\sigma^2}} \quad . \quad (20)$$

Equation (18) can be fitted to experimental data directly using nonlinear fitting. However, to ensure convergence, it is convenient guess a relatively narrow distribution function $\theta(\tau)$ first, and then make the fit. Further iterations are then made until the best possible fit is obtained. When needed, more complicated fitting functions and procedures can be considered, as detailed in e.g. Ref. [59]. However, for the two supercapacitors considered in the current study, it is found that Gaussian distribution function is sufficient since the deviations from the Randles circuit are not large.

The black and blue data points in Fig. 5 a) and b) show the modulus and phase of the measured impedance data for supercapacitors A and B, respectively. The dashed red lines in Fig. 6 a) and b) show the fit of Eqs. (18) and (20) to the experimental data with $R_s=5.7$ m Ω , $R_p=6.4$ Ω , $C_p=342.6$ F, $\tau_0=2193$ s, $\sigma=10$ s

and $L=141$ nH. The dashed green lines in in Fig. 6 a) and b) show the fit of Eq. (18) and (20) to the experimental data with $R_s=38.3$ m Ω , $R_p=67.3$ Ω , $C_p=11.3$ F, $L=143$ nH, $\tau_0=760$ s and $\sigma=10$ s.

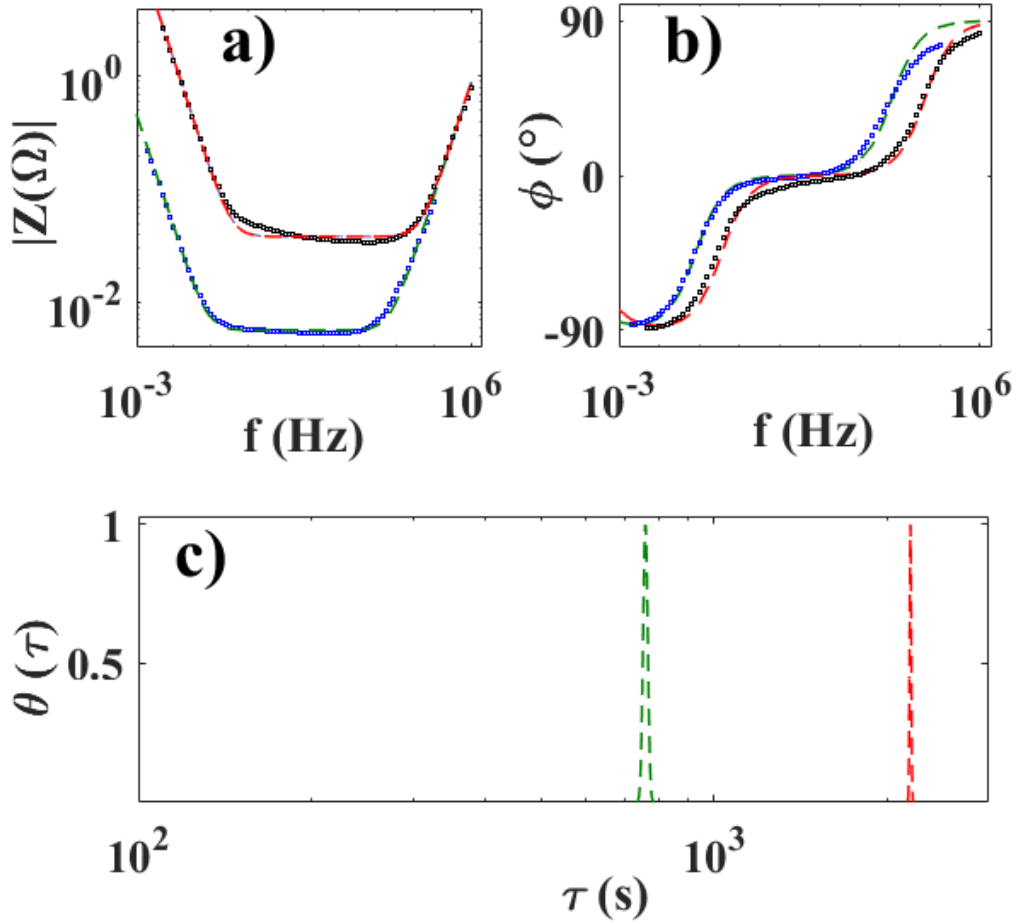


Figure 6. Figure a) and b) show the modulus $|Z|$ and phase angle ϕ obtained using impedance spectroscopy, respectively. The black experimental data points correspond to supercapacitor A, whereas the blue data points correspond to supercapacitor B. The red and dashed lines are the fits of Eqs. (18) and (20) to the experimental data for supercapacitor A and B, respectively. The corresponding distribution of relaxation times are shown in c), with peaks at $\tau_0=760$ s and $\tau_0=2193$ s for supercapacitors A and B.

The impedance spectrum can be well described by the simple model used here, with two very narrow gaussian peaks in the distribution function at $\tau_0=760$ s for supercapacitor A and $\tau_0=2193$ s for supercapacitor B. To this end, it should be recalled that a relaxation time of 2200 s was obtained when galvanostatically charging supercapacitor B at 0.5 A, which is consistent with the data obtained using impedance spectroscopy. In the case of supercapacitor A, galvanostatic charging at 0.1 A gave a relaxation time of 700 s, while charging at 0.8 A gave 85 s. From impedance spectroscopy one obtains $\tau_0=760$ s, which is consistent with the number obtained for the slowest charging. This is not unexpected, since the relaxation time is extracted from the low-frequency part of the impedance spectrum, corresponding to slow processes. Nonetheless, it should also be emphasized that self-discharge provides even larger relaxation times within this model.

7. Discussion

The aim of this study was to demonstrate that the dynamic equivalent circuit can be used to model the behavior of supercapacitors if one allows for an interpretation in terms of a distribution of relaxation times. Galvanostatic charging with weakly nonlinear behavior is found to be well described using this method, but only a single effective relaxation time can be extracted. On the other hand, self-discharging of supercapacitors exhibits a wide distribution of relaxation times, with large relaxation times playing a major role. Impedance spectroscopy utilizes weak excitations about a working point and is rather well described by an elemental circuit branch consisting of a resistor in parallel with a capacitor, and the distribution of relaxation times is therefore narrow.

It should be pointed out that in principle there could be one relaxation time for each electrolyte-filled pore in the porous carbon, thus requiring a very large number of branches to fit the experimental data if a very good overlap between theoretical and experimental data is needed. Using a discrete equivalent circuit under such conditions might require unnecessary large computational efforts. In fact, it might be more

convenient to find a continuous distribution of relaxation constants if such a distribution can be calculated efficiently without large computational efforts. One may utilize existing databases (e.g. [44]) to obtain distributions of relaxation times as was done for self-discharging supercapacitors (Fig. 4b and 5b), thus minimizing computational time.

The question of uniqueness of the relaxation time distribution is an important and mathematically very challenging question. For very narrow distributions, like the one obtained from the impedance spectrum (Fig. 6b), one expects that the representation is close to unique, due to the fact that large changes from the obtained distribution would most likely also result in large changes in the theoretical functions for the impedance. On the other hand, for the self-discharging curves (Fig. 4b and 5b) there are other possible functions except the stretched exponential function that can be used, thus allowing other distributions as well. However, it should be noted that since the experimental curves in Fig. 4 a) and 5 a) have non-exponential shapes with a fast initial phase followed by a prolonged decay, one must expect a wide distribution of relaxation times for any distribution that is to represent self-discharge. Since the stretched exponential function has found success in a wide variety of other fields of physics [45], it makes sense to utilize this function to extract the distribution of relaxation times using existing data bases [44].

In the current work, the method for validation of the distribution of relaxation time is by observing how well the method allows one to fit theoretical curves to experimental data. However, since this is not really a microscopic justification, further studies are needed. Future work could be aimed at validating the distribution of relaxation times obtained using the method proposed here. While experiments have been conducted to characterize relaxation of single channels [60], few experiments have been done to characterize the relaxation of a distribution of channels with known porous properties. This lack of available techniques on the micro and nanoscale makes it hard to obtain a direct correlation with the macroscopic distribution function. Further validation could be obtained by comparison with numerical

modelling [61], however such efforts are very computationally challenging if they are to be based on x-ray tomographic images of real porous carbon structures.

8. Conclusion

This study presents a method to model supercapacitors in both time and frequency domains using a dynamic equivalent circuit model with a continuous distribution of time constants. The model was used to monitor the charging and discharging of supercapacitors, the self-discharge as well as the impedance spectrum. Only one type of equivalent circuit is needed to model the supercapacitor in a consistent manner. While self-discharge could be modelled using a broad distribution of relaxation times, other charging and discharging procedures were found to be fitted well with a narrow distribution.

It should be emphasized that the physical behavior of other supercapacitors or even pseudocapacitors could be interpreted in terms of a distribution of relaxation times as described here. It is therefore anticipated that the model presented here could be a valuable diagnostic tool when studying such energy storage systems.

REFERENCES

- (1) H. I. Becker, U.S. pat., 2800.616 to General Electric Co., **1957**.
- (2) B. E. Conway, *Electrochemical Supercapacitors*, Kluwer Academic, New York, USA, 1999.
- (3) R.L. Spyker and R.M. Nelms, “Classical equivalent circuit parameters for a double-layer capacitor”, *IEEE Trans. Aerosp. Electron. Syst.*, 36, **2000**, 829–36.
- (4) L. Zubieta and R. Bonert, “Characterization of double-layer capacitors for power electronics applications”, *IEEE Trans. Ind. Appl.*, 36, **2000**, 199–205.
- (5) H. Gualous, D. Bouquain, A. Berthon and J.M. Kauffmann, “Experimental study of supercapacitor serial resistance and capacitance variations with temperature”, *J. Power Sources*, 123, **2003**, 86–93.
- (6) F. Rafika, H. Gualous, R. Gallay, A. Crausaz and A. Berthon, “Frequency, thermal and voltage supercapacitor characterization and modeling. *J Power Sources*, 165, **2007**, 928–934.
- (7) R. Faranda, “A new parameters identification procedure for simplified double layer capacitor two-branch model”, *Electr. Power Syst. Res.* 80, **2010**, 363–71.
- (8) S. Fletcher, V.J. Black and I. Kirkpatrick, “A universal equivalent circuit for carbon-based supercapacitors”, *J. Solid State Electrochem.*, 18, **2014**, 1377-1387.
- (9) P.O. Logerais, M.A. Camara, O. Riou, A. Djellad, A. Omeiri, F. Delaleux and J.F. Durastanti, “Modeling of a supercapacitor with a multibranch circuit”, *Int. J. Hydrogen Energy*, 40, **2015**, 13725–13736.
- (10) R. Chai, and Y. Zhang, “A practical supercapacitor model for power management in wireless sensor nodes”, *IEEE Trans. Power Electron.*, 30, **2015**, 6720–6730.
- (11) A. Weddell, G. Merrett, T. Kazmierski and B. Al-Hashimi, “Accurate supercapacitor modeling for energy harvesting wireless sensor nodes”, *IEEE Trans, Circuits Syst, II Exp Briefs*, 58, **2011**, 911–915.

- (12) Y. Zhang and H. Yang, “Modeling and characterization of supercapacitors for wireless sensor network applications”, *J. Power Sources*, 196, **2011**, 4128–4135.
- (13) H. Yang and Y. Zhang, “A study of supercapacitor charge redistribution for applications in environmentally powered wireless sensor nodes”, *J. Power Sources*, 273, **2015**, 223-236.
- (14) H. Yang and Y. Zhang, “Characterization of supercapacitor models for analyzing supercapacitors connected to constant power elements”, *J. Power Sources*, 312, **2016**, 165-171.
- (15) K. Liu, C. Zhu, R. Lu and C.C. Chan, “Improved study of temperature dependence equivalent circuit model for supercapacitors”, *IEEE Trans. Plasma Sci.*, 41, **2013**, 1267–1271.
- (16) S. Buller, E. Karden, D. Kok and R. Doncker, “Modeling the dynamic behavior of supercapacitors using impedance spectroscopy”, *IEEE Trans. Ind. Appl.*, 38, **2002**, 1622–6.
- (17) Y. Parvini Y, J.B. Siegel, A.G. Stefanopoulou and A.Vahidi, “Supercapacitor electrical and thermal modeling, identification, and validation for a wide range of temperature and power applications”, *IEEE Trans. Ind. Electron.*, 63, **2016**, 1574–1585.
- (18) R. DeLevie, “On porous electrodes in electrolyte solutions”, *Electrochim. Acta*, 8, **1963**, 751-780.
- (19) C. Pean, B. Rotenberg, P. Simon and M. Salanne, “Multi-scale modelling of supercapacitors: From molecular simulations to a transmission line model”, *J. Power Sources*, 326, **2016**, 680-685.
- (20) J. Black and H.A. Andreas, “Effects of charge redistribution on self-discharge of electrochemical capacitors”, *Electrochim. Acta*, 54, **2009**, 3568-3574.
- (21) S.H. Kim, W. Choi, K.B. Lee and S. Choi, “Advanced dynamic simulation of supercapacitors considering parameter variation and self-discharge” *IEEE Trans. Power Electron.*, 26, **2011**, 3377-3385.
- (22) M. Kroupa, G.J. Offer and J. Kosek, “Modelling of supercapacitors: Factors influencing performance”, *Journal of the Electrochemical Society*, 163, **2016**, A2475-A2487.

- (23) R. Drummond, S. Zhao, D.A. Howey and S.R. Duncan, “Circuit synthesis of electrochemical supercapacitor models”, *J. Energy Storage*, 10, **2017**, 48-55.
- (24) N. Devillers, S. Jemei, M.C. Péra, D. Bienaimé and F. Gustin, “Review of characterization methods for supercapacitor modelling”, *J. Power Sources*, 246, **2014**, 596-608.
- (25) L. Zhang L, Z. Wang Z, X. Hu, F. Sun and D.G. Dorrell, “A comparative study of equivalent circuit models of ultracapacitors for electric vehicles”, *J Power Sources*, 274, **2015**, 899–906.
- (26) I.N. Jiya, N. Gurusinge and R. Gouws, “Electrical circuit modelling of double layer capacitors for power electronics and energy storage applications: A review”, *Electronics*, 7, **2018**, 268.
- (27) Q.A. Huang, Y. Li, K.C. Tsay, C. Sun, C. Yang, L. Zhang and J. Zhang, “Multi-scale impedance model for supercapacitor porous electrodes: Theoretical prediction and experimental validation”, *J. Power Sources*, 400, **2018**, 69-86.
- (28) V. Musolino, L. Piegari and E. Tironi, “New full-frequency-range supercapacitor model with easy identification procedure”, *IEEE Trans. Ind. Electron* 60, **2013**, 112–120.
- (29) D. Torregrossa, M. Bahramipناه, E. Namor, R. Cherkaoui and M. Paolone, “Improvement of dynamic modeling of supercapacitor by residual charge effect estimation”, *IEEE Trans. Ind. Electron*, 61, **2014**, 1345–1354.
- (30) N. Rizoug, P. Bartholomeüs and P. Moigne, “Modeling and characterizing supercapacitors using an online method”, *IEEE Trans. Ind. Electron.*, 57, **2010**, 3980–3990.
- (31) L. Zhang, Z. Wang, F. Sun and D.G. Dorrell, “Online parameter identification of ultracapacitor models using the extended Kalman filter”, *Energies*, 7, **2014**, 3204–3217.
- (32) L. Zhang, X. Hu, Z. Wang, F. Sun and D.G. Dorrell, “A review of supercapacitor modeling, estimation, and applications: A control/management perspective”, *Renewable and Sustainable Energy Reviews*, 81, **2018**, 1868-1878.

- (33) C. Liu, Y. Wang, Z. Chen and Q. Ling, "A variable capacitance based modeling and power capability predicting method for ultracapacitor", *J. Power Sources*, 374, **2018**, 121-133.
- (34) V.V. Uchaikin, R.T. Sibatov and S.A. Ambrozevich, "Comment on: Review of characterization methods for supercapacitor modelling", *J. Power Sources*, 307, **2016**, 112-113.
- (35) A.S. Ambrozevich, S.A. Ambrozevich, R.T. Sibatov and V.V. Uchaikin, "Features of charging-discharging of supercapacitors", *Russian Electrical Engineering*, 89, **2018**, 73-80.
- (36) C. Zou, L. Zhang, X. Hu, Z. Wang, T. Wik and M. Pecht, "A review of fractional-order techniques applied to lithium-ion batteries, lead-acid batteries, and supercapacitors", *J. Power Sources*, 390, **2018**, 286-296.
- (37) A. Allagui, T.J. Freeborn, A.S. Elwakil, M.E. Fouda, B.J. Maundy, A.G. Radwan, Z. Said and M.A. Abdelkareem, "Review of fractional-order electrical characterization of supercapacitors", *J. Power Sources*, 400, **2018**, 457-467.
- (38) S. Fletcher, I. Kirkpatrick, R. Dring, R. Puttock, R. Thring and S. Howroyd, "The modelling of carbon-based supercapacitors: Distributions of time constants and Pascal Equivalent circuits", *J. Power Sources*, 345, **2017**, 247-253.
- (39) A. Oz, D. Gelman, E. Goren, N. Shomrat, S. Baltianski and Y. Tsur, "A novel approach for supercapacitors degradation characteristics", *J. Power Sources*, 355, **2017**, 74-82.
- (40) K.B. Li, D.W. Shi, Z.Y. Cai, G.L. Zhang, Q.A. Huang, D. Liu and C.P. Yang, "Studies on the equivalent serial resistance of carbon supercapacitor", *Electrochim. Acta*, 174, **2015**, 596-600.
- (41) H. Yang, "Application of Peukert's law in supercapacitor discharge time prediction", *J. Energy Storage*, 22, **2019**, 98-105.

- (42) R. Kolrausch, "Theorie des elektrischen Rückstandes in der Leidener Flasche", *Ann. Phys.*, 167, **1854**, 56-82.
- (43) G. Williams and D.C. Watts, "Non-symmetrical dielectric relaxation behaviour arising from a simple empirical decay function", *Trans. Faraday Soc.*, 66, **1970**, 80-85.
- (44) M. Dishon, J.T. Bendler and G.H. Weiss, "Tables of the inverse Laplace transform of the function $\exp(-s^\beta)$ ", *Journal of Research of the National Institute of Standards and Technology*, 95, **1990**, 433-467.
- (45) D.C. Johnston, "Stretched exponential relaxation arising from a continuous sum of exponential decays", *Phys. Rev. B*, 74, **2006**, 184430.
- (46) V. Sedlakova, J. Sikula, J. Mazner, P. Sedlak, T. Kuparowitz, B. Buegler and P. Vasina, "Supercapacitor equivalent circuit model based on charges redistribution by diffusion", *J. Power Sources*, 286, **2015**, 58-65.
- (47) B.E. Conway, W.G. Pell and T-C. Liu, "Diagnostic analyses for mechanisms of self-discharge of electrochemical capacitors and batteries", *J. Power Sources*, 65, **1997**, 53-59.
- (48) A.M. Oickle, J. Tom and H.A. Andreas, "Chemical oxidation and its influence on self-discharge in aqueous electrochemical capacitors", *Carbon*, 110, **2016**, 232-242.
- (49) J. Black and H.A. Andreas, "Predictions of the self-discharge profile of an electrochemical capacitor electrode in the presence of both activation-controlled discharge and charge redistribution", *J. Power Sources*, 195, **2010**, 929-935.
- (50) M. Kaus, J. Kowal and D.U. Sauer, "Modelling the effects of charge redistribution during self-discharge of supercapacitors", *Electrochim. Acta*, 55, **2010**, 7516-7523.

- (51) A. Lewandowski, P. Jakobczyk, M. Galinski and M. Biegun, "Self-discharge of electrochemical double layer capacitors", *Phys. Chem. Chem. Phys.*, 15, **2013**, 8692.
- (52) C. Hao, X. Wang, Y. Yin and Z. Hou, "Analysis of charge redistribution during self-discharge of double-layer supercapacitors", *J. Electron. Mater.*, 45, **2016**, 2160-2170.
- (53) J.W. Graydon, M. Panjehshahi and D.W. Kirk, "Charge redistribution and ionic mobility in the micropores of supercapacitors", *J. Power Sources*, 245, **2014**, 822-829.
- (54) T. Tevi, H. Yaghoubi, J. Wang and A. Takshi, "Application of poly(p-phenylene oxide) as a blocking layer to reduce self-discharge in supercapacitors", *J. Power Sources*, 241, **2013**, 589-596.
- (55) T. Tevi and A. Takshi, "Modeling and simulation study of the self-discharge in supercapacitors in presence of a blocking layer", *J. Power Sources*, 273, **2015**, 857-862.
- (56) A. Laheäär, A. Arenilas and F. Béguin, "Change of self-discharge mechanism as a fast tool for estimating long-term stability of ionic liquid based supercapacitors", *J. Power Sources*, 396, **2018**, 220-229.
- (57) J.F. Shen, Y.J. He and Z.F. Ma, "A systematical evaluation of polynomial based equivalent circuit for charge redistribution dominates self-discharge process in supercapacitors", *J. Power Sources*, 303, **2016**, 294-304.
- (58) R.M. Fuoss and J.G. Kirkwood, "Electrical properties of solids. VIII. Dipole moments in polyvinyl chloride-diphenyl systems", *J. Am. Chem. Soc.*, **1941**, 63, 385.
- (59) B.A. Boukamp, "Fourier transform distribution function of relaxation times; application and limitations", *Electrochimica Acta*, **2015**, 154, 35-46.
- (60) R. Tivony, S. Safran, P. Phincus, G. Silbert and J. Klein, "Charging dynamics of an individual nanopore", *Nature Commun.*, **2018**, 9, 4203.

- (61) M. Salanne, B. Rotenberg, K. Naoi, K. Kaneko, P.L. Taberna, C.P. Grey, B. Dunn and P. Simon, “Efficient storage mechanisms for building better supercapacitors”, *Nature Energy*, **2016**, 1, 16070.